EFDA–JET–CP(12)06/34

M.-L. Mayoral, V. Bobkov, A. Czarnecka, I. Day, A. Ekedahl, P. Jacquet, M. Goniche, R. King, K. Kirov, E. Lerche, J. Mailloux, D. Van Eester, O. Asunta, C. Challis, D. Ciric, J.W. Coenen, L. Colas, M.C. Giroud, M. Graham, I. Jenkins, E. Joffrin, T. Jones, D. King, V. Kiptily, C.C. Klepper, C. Maggi, F. Marcotte, G. Matthews, D. Milanesio, I. Monakhov, M. Nightingale, R. Neu, J. Ongena, T. Pütterich, V. Riccardo, F. Rimini, J. Strachan, E. Surrey, V. Thompson, G. Van Rooij and JET EFDA contributors

On the Challenge of Plasma Heating with the JET Metallic Wall

On the Challenge of Plasma Heating with the JET Metallic Wall

M.-L. Mayoral[1], V. Bobkov[2], A. Czarnecka[3], I. Day[1], A. Ekedahl[4], P. Jacquet[1], M. Goniche[4], R. King[1], K. Kirov[1], E. Lerche[5], J. Mailloux[1], D. Van Eester[5], O. Asunta[6], C. Challis[1], D. Ciric[1], J.W. Coenen[7], L. Colas[4], M.C. Giroud[1], M. Graham[1], I. Jenkins[1], E. Joffrin[4], T. Jones[1], D. King[1], V. Kiptily[1], C.C. Klepper[8], C. Maggi[2], F. Marcotte[9], G. Matthews[1], D. Milanesio[10], I. Monakhov[1], M. Nightingale[1], R. Neu[2], J. Ongena[5], T. Pütterich[2], V. Riccardo[1], F. Rimini[1], J. Strachan[11], E. Surrey[1], V. Thompson[1], G. Van Rooij[12] and JET EFDA contributors*

JET-EFDA, Culham Science Centre, OX14 3DB, Abingdon, UK

[1]EURATOM-CCFE Fusion Association, Culham Science Centre, OX14 3DB, Abingdon, OXON, UK
[2]Max-Planck-Institut für Plasmaphysik, EURATOM Association, Garching, Germany
[3]Association EURATOM-IPPLM, Hery 23, 01-497 Warsaw, Poland
[4]CEA, IRFM, F-13108 St-Paul-Lez-Durance, France.
[5]Association "EURATOM - Belgian State", ERM-KMS, TEC partners, Brussels, Belgium
[6]Aalto University, Association EURATOM-Tekes,, FIN-00076 Aalto, Finland
[7]Institute of Energy and Climate Research, Assoc EURATOM-FZJ, Jülich, German,
[8]Oak Ridge National Laboratory, Oak Ridge, TN 37831-6169, USA
[9]École Nationale des Ponts et Chaussées, F77455 Marne-la-Vallée, France.
[10]Associazione EURATOM-ENEA sulla Fusione, Politecnico di Torino, Italy
[11]PPPL, Princeton University, Princeton, USA
[12]DIFFER, Association EURATOM-FOM, TEC partners, Netherlands,
** See annex of F. Romanelli et al, "Overview of JET Results",*
(24th IAEA Fusion Energy Conference, San Diego, USA (2012)).

Preprint of Paper to be submitted for publication in Proceedings of the
24th IAEA Fusion Energy Conference (FEC2012), San Diego, USA
8th October 2012 - 13th October 2012

ABSTRACT.
In this paper, the major aspects linked to the use of the JET heating systems: NBI, ICRF and LHCD, in the new JET ITER-like wall (ILW) are presented. We show that although there were issues related to the operation of each system, efficient and safe plasma heating was obtained with room for higher power. For the NBI up to 25.7MW was safely injected; issues that had to be tackled were mainly the beam shine through and beam re-ionisation before entrance in the plasma. For the ICRF system, 5MW were coupled in L-mode and 4MW in H-mode; the main areas of concern were RF-sheaths related heat loads and impurities production. For the LH, 2.5MW were delivered without problems; arcing and generation of fast electron beams in front of the launcher that can lead to high heat loads were the keys issues. For each system, an overview will be given of: their compatibility with the new metallic wall, the main modifications implemented for a safe use, the differences in behavior compared with the previous wall in carbon, with special emphasis on heat loads and impurity content in the plasma.

1. INTRODUCTION

In the JET tokamak, the plasma heating and current drive (see Fig.1) is provided by:

- Neutral Beam Injection (NBI) consisting of two neutral beam injector boxes (NIBs) each equipped with 8 Positive Ion Neutral Injectors (PINIs) [1]. 4 PINIs in each NIB are grouped into a tangential bank and 4 in a normal bank. 4 PINIs in each NIB can be steered between two positions relative to the usual plasma centre (upshifted and standard). The latest system upgrade [2] launched in spring 2005 and concluded during the 2011-12 JET experimental campaigns, had three main goals: (a) to increase the total injected deuterium (D) neutral beam power from 24MW to 34MW (with 125kV/2.1MW per PINI); (b) to increase the NBI pulse duration at maximum power from the present 10s to 20s, and at half power from 20s to 40s; (c) to improve the availability and reliability of the NBI system.
- An ion cyclotron resonance frequency (ICRF) system with 4 A2 antennas [3] operating between 25 and 51MHz. Waves with symmetric spectra ("dipole" phasing; parallel wave number $k_{||} \sim 6.6m^{-1}$) or asymmetric spectra ("$\pm 90^{o}$" phasing, $|k_{||}| \sim 3.3m^{-1}$) are launched by adjusting the phase difference in between the 4 straps of each antenna. The issue of operation on ELMy H-mode was solved in the past few years with the implementation of ELM tolerant systems and up to 7MW was coupled in 2009 on type I ELMy H-mode [3-4]. For standard operations (fully conditioned antenna, Radial Outer Gap (ROG) ~5cm), power levels in the range of 5MW (33MHz) to 10MW (>42MHz) in L-mode and 3MW (33MHz) to 6MW (42MHz) in H-mode, can be expected but note that record power levels of 16.7MW/0.3s (Pulse No: 38049) and 14.6MW/1s (Pulse No: 39960) were obtained with 3cm ROG, 51MHz in dipole phasing. The ITER-like ICRF antenna [6], out of operation since mid-2009 due to a broken capacitor, was not used so far with the JET ILW.
- A lower hybrid current drive (LHCD) system [7-8] operating at 3.7GHz. The launcher

integrates 48 multi-junctions modules fed by 24 klystrons. The usual radiated $n_{||}$ spectrum is peaked at 1.84 (values between 1.4 and 2.3 can be used). For standard operation (fully conditioned launcher, ROG ~ 5cm), power level in the range of 5MW in L-mode and 3MW in Hmode, can be expected. Record power levels of 7.3MW/0.2s (Pulse No: 33618), 6.2MW/2s (Pulse No: 34419) were obtained in L-mode and up to 3.2MW with a 13cm ROG was coupled in Hmode [9]. D_2 gas is injected from the module GIM6 (~1m from the launcher) when the coupling needs to be improved.

In this paper, a review is given of the compatibility of the NBI, ICRF and LH systems with the JET ITER–like wall (ILW) [10] made of W or W-tile for the divertor and of mainly Be or Be/coated tiles for the main chamber (see Fig.1). It includes a description of the heating systems modifications for safe operation in a metallic environment and of the adjustments made to the new wall design for safe application of high heating power. Operational issues (heat loads and impurities in the plasma) directly linked to the use of the heating systems and encountered in the first campaign after the ILW installation are presented.

2. NEUTRAL BEAM INJECTION

2.1. MODIFICATIONS FOR OPERATION IN THE ILW

In parallel with the ILW installation, the EP2 upgrade of the NBI system was completed [22]. All the PINIs (previously 80kV/52-60A tetrodes PINIs and 130kV/58A triode PINIs) were converted to triode EP2 PINIs (125kV/65A in D). The conversion consisted mainly of an ion source modification from supercup to chequerboard type producing more molecular ions, which are easier to neutralize, and a reoptimisation of the accelerators to increase the beam current. Some beam-line components were also modified to cope with an increase by cups a factor four in the fractional and molecular residual ion power. In addition the inertial duct liners were replaced by actively cooled liners ones. Finally, half of the High Voltage Power Supplies (HVPS) were replaced. Because of the increase in the beam center power density and in the pulse length capabilities, particular care was given to the design of the plasma facing components (PFCs) possibly interacting with neutrals injected from the new PINIs. Prior to the full use in the ILW environment, EP2 PINIs were tested on the JET Neutral Beam (NB) test bed and two were installed in 2009 on the tokamak to measure the injected beam power and to confirm that the power loads on various beam-line components were within the predicted margins (see [11]). The NB shine-through was inferred from measurements on the test bed. At 125kV, it was found that peak power densities in the range of 48MW/m^2 could be expected on the inner wall and up to 24MW/m^2 on the outer wall and it was decided to use for areas at risk, W-coated CFC tiles both on the inner wall (with the W-coated IWGL recessed by 2.5cm compared to Be tiles) and on the outer wall (at the top and bottom of the ICRF antennas A and C) (see Fig.2). In addition, an upgraded real-time protection, based on bulk and surface temperature modeling was developed in order to maximize the use of the new NBI power capabilities over a broad range of densities and plasma configurations while staying within the allowed W-coating temperature limit,

initially set to 1200°C. Finally, a fraction of the injected neutrals can be ionised in the plasma edge outside the separatrix, drift and then impinge on specific areas of the outer wall referred to as the beam "re-ionisation" tiles (against PL8B and PL4B – see Fig.1). Following estimations [12] that the power density for 8 PINIs at high density (1.10^{20} m^{-3}) for 130kV D beams could be in the range of 5.5 to 23MW/m^2 for 8 to 5cm ROG, these tiles were also made of W-coated CFC.

2.2. OPERATIONAL EXPERIENCE WITH THE ILW

A phased approach was taken to increase the NBI power during initial ILW operation and for the commissioning of the new power supplies. The voltage was slowly increased from 80kV (~1MW/PINI) to 100kV (~1.5MW/PINI). Once PEWS2 was commissioned, operation at lower plasma density became possible and as the new HVPS came on line, the injected power could be increased routinely to the 20MW level. A record power of 25.7MW was obtained at the end of the campaign using 14 PINIs at voltages from 92 to 117kV. 4MW of NBI power (at 80kV) was applied for 15s using the extended pulse length capability of the EP2 upgrade. The new actively cooled duct liners were able to achieve steady state temperatures (150-200°C) with no operational limitation. No increase in the impurity levels (expect a minor increase in copper) could be related to application of the NBI power. Particular attention was given to the monitoring of any increase in W due to sputtering of W-coated CFC tiles by fast D neutrals but no evidence of a W source in the main chamber due to NBI was found. This is in agreement with pre-campaigns modelling [13], which had shown that the magnitude of the sputtering would not lead to significant W plasma radiation. Hot- spots on the beam reionisation tiles were observed using one of the cameras from the Protection of the ITER-Wall (PIW) system [14] which views the re-ionisation tiles adjacent to PL4B. An example image is shown on Fig.3, where localised hot-spots are seen during a limiter pulse on the outer wall heated with 5MW of NBI. The effect of the edge plasma density on these hot-spots (for a given ROG), is shown on Fig.4. Both shown ELMy H-modes were performed at the same magnetic field (2.6T), plasma current (1.6MA) and ROG (7cm) and differed only by the gas injection level. In PulseNo: 81560, the density was slowly raised until a hotspot appeared on the re-ionisation tile leading to the termination of the pulse by the protection system. Note that the maximum temperature set by the PIW was very conservative. Future work includes the estimation of the related power densities. Finally, no issues due to possible NBI fast ions losses on the outer wall were observed, in agreement with ASCOT simulation [15] that had predicted only very small losses (<1‰) with lost power in the kW range and heat loads in the W/m^2 range.

3. ION CYCLOTRON RESONANCE FREQUENCY HEATING

3.1. MODIFICATIONS FOR OPERATION IN THE ILW

All the plasma facing components (PFCs) around the A2s ICRF antennas (top and bottom horizontal bars, antenna septum) were replaced [16], with the exception of the antenna screen bars already made of Be. The septa are now recessed by 8mm to the neighbouring PL (4 to 7mm before) with

a slightly modified shape aimed at reducing the thermal loads. New flux excluders in Cu-coated Inconel were fitted between the antennas and the PL to provide a path for the antenna strap mirror currents. Unfortunately, the flux excluder between the antenna B and PL3B was not positioned correctly and it was decided that no current should be applied to B4 strap until the flux excluder is repositioned. Because of the system configuration this meant not using half of antenna B (B3/B4) and the loss of the ELM tolerance from half of A (A3/A4) [3]. During the present shutdown, newly designed flux excluder will be fitted to allow the full ICRF power capabilities to be exploited.

3.2. OPERATIONAL EXPERIENCE WITH THE ILW

3.2.1 Power, coupling and heating efficiency.

A careful increase of the antenna voltage was performed alternating vacuum and plasma conditioning pulses in order to monitor any 'abnormal' arcing behaviour or antenna performance changes. Maximum voltages on the transmission line, Vmax, up to 30kV were reached at 33, 42, 47 and 51MHz without issues. Up to 5MW of ICRF power was coupled (Pulse No: 81313, 42MHz, dipole phasing, 4cm ROG) with Vmax up to 25kV, i.e. far from any power limit (for constant loading, $P_{ICRF} \propto V_{max}^2$). Because of the lowered L to H power threshold with the ILW compared to the C-wall [17], this pulse as most of the pulses with more than 3 MW, magnetic fields <2.7T and densities <3 10^{19} m^{-3} was already an H-mode. In type I ELMy H-modes, 4MW was coupled (Pulse No: 83398, 42MHz, dipole phasing, 5cm ROG) with Vmax from 20 to 30kV (depending on transmission lines). This means that, with the 4 antennas, under similar condition up to 6MW should be available for the next campaign. Difference in antenna loading between the C-wall and ILW, including the effects of lower recycling, was difficult to characterize as no matching pulses, with measurements of scrape-off-layer (SOL) density profiles critical for the loading value [4] could be obtained. A statistical analysis showed that the loading of antennas A and B tends to be lower with the ILW, but no clear difference was observed for C and D. Besides any change in the SOL density for a given ROG, the lower coupling on A and B could be explained by changes in the poloidal limiter position between antennas A and B (PL2B and PL2D, see Fig.1, are now 3.5mm behind the other PLs compared to zero before) and more probably by the operation with two straps, leading to a broader antenna spectrum. This will be further investigated using the recently developed TOPICA modelling [18] of the A2s antennas. So far only on-axis or off-axis H minority heating in D was used, with H levels in the 5% range to ensure good single-pass absorption. Increases in electron central temperature, T_e, up to 0.85keV/MW were obtained, which is slightly lower than C-wall values (up to 1keV/MW), but increase in energy content was found similar (~0.2 MJ/MW) [19]. An example of efficient ICRF plasma heating is shown on FIG.6 where, additionally to the increase in T_e, lengthening of sawtooth periods, characteristic of centrally peaked fast H ions pressure [20] was observed. Heat loads. A concern when using the ICRF antennas with the new wall was local heat loads on surrounding Be limiters and antenna septum due to the acceleration of ions in the RF sheath rectified voltages created by the residual parallel electric field on the antenna structure [22] and observed previously

on Tore Supra [23] and on JET with the C-wall [24]. Infra-Red (IR) thermography and a thermal model for the ILW Be tiles, was used to further characterise these heat fluxes [25]. As expected from RF-sheath theory, higher fluxes are obtained for asymmetric phasing ($\pm 90^o$) compared with dipole phasing. The maximum value obtained was 4.5MW/m^2 (flux normal to antenna A septum) when 2MW/antenna was coupled using -90^o phasing with a 4cm ROG. During the experimental campaign, the related hot-pots monitored by the PIW viewing system, never get close to the design limits (6MW/m^2 for 10s) and did not limit operation (temperature limit set at 950^{o}C ~ 4MW/m2 for 10s) as typical ICRF pulse durations were below 10s and mainly dipole phasing was used.

3.2.2 Plasma impurity content.

During ICRF heating, the bulk radiated power was found to increase significantly compared to C-wall operation. For Pulse No: 81852 (Fig.6), the effect of 3.5MW of either central ICRF or NBI heating were compared (the ohmic power was ~ 1.8MW). During the ICRF phase, ~ 50% of the power was radiated from the plasma bulk compared with ~ 35% in the NBI phase. The main radiators during ICRF were identified as W and Ni. The W concentration was found hollow for the ICRF (2.10^{-4} at ρ~0.25 and 4.10^{-4} at ρ~0.6). The increase in Ni during ICRF, consistent to C-wall observations [26], was estimated to contribute to the bulk radiation up to a level of 20% [27]. The Be level also increased during the ICRF heating. Monitoring of the Be line intensity with line of sight directed on the Faraday screen of the D4 strap and on PL7B, was performed [28]. Quite interestingly, a bigger increase in Be was observed from the D4 sightline when the antenna C was in use. A possible explanation for this local increase is an enhanced Be sputtering due to connection to high RF sheath potential areas.

3.2.3 Heavy impurity sources

Two obvious possible W sources are the divertor and its entrance (top of tiles 8, tiles B and C - Fig.1) which can be magnetically connected to ICRF antennas. The analysis of the WI emission (representing the W source at the surface) from the divertor, tile 8 and B, was done in detail for #81852 at two toroidal locations [29]. FIG.7 shows that the WI emission averaged over the constant heating phase was slightly higher during NBI than during ICRF. Other W-sources were then needed to explain the difference in cW see on Fig.6. It is important to mention that by toggling between different antennas, q_{95} and antenna phasing, the sign of a specific interaction between ICRF antennas and the top of tile 8, was observed (with W fluxes below the $10^{17}m^{-2}s^{-1}$ range) and it is reasonable to think that divertor entrance tiles C (unfortunately not visible by any diagnostics), might be a source of W. Interactions with main chamber W-coated tiles (shine through areas, restraint rings - see Fig.1) were also considered, particularly as it was found that limiter pulses specifically designed to minimise contact with the W divertor, had higher W levels when heated with ICRF compared with NBI. Evidence of aninteraction with the main chamber was found by doing overnight Be evaporation. Comparing Pulse No: 83383 prior to the Be evaporation with Pulse No: 83428 (Fig.8), the first pulse

after the evaporation, one could clearly see a strong reduction in Ni-line signal and in the radiated power (~45%). Unfortunately, quantitative changes in W content could not be deduced in these pulses due to a diagnostic failure. Note that the W-line emission from midplane VUV spectroscopy, shown on Fig.8, suffers from Ni contamination. Nevertheless, a W decrease was plausible because the decrease in the Prad could not be explained by the Ni decrease alone. Note that the Be layer deposited (~3nm) was expected to disappear very quickly (~ 1 pulse) in areas in direct contact with the plasma. The fact that after 11 ELMy H mode pulses, the radiation level in Pulse No: 83442 was still lower than in Pulse No: 83383 prior to the evaporation, indicating a source of impurities from W-coated and Inconel recessed areas

3.2.4 Factor influencing the W and Ni level.

The first parameter strongly influencing the W and Ni levels is the plasma edge density. This was shown for W in [29][30], for Ni in the ILW [27] and in the C-wall [26], and can be due to a number of different processes: decrease of the impurity source; change in mean free path of the sputtered impurity neutrals and in plasma transport properties, giving reduced impurity confinement and direct dilution of the impurities in the plasma. Another parameter that affects the impurity content is the phasing of the ICRF antenna, with $\pm 90^{o}$ leading to higher Ni [27] [31] and higher W emission from on the divertor baffle [29]. During scans in H level (H%) up to 30%, a drop in radiation accompanied by a drop in cW and in Be and Ni emission was observed, with a minimum around 20%. Interestingly, the net heating efficiency only slightly decreased for H% < 20%. As H% was further increased, the radiation started to rise, probably due to the strong drop in heating efficiency (see [19]). The production of impurities during ICRF is not a new phenomenon [31-32], and is generally attributed to acceleration of light impurities in the RF-rectified potentials [22], enhancing the sputtering from metallic components. Recent modelling of the A2 antennas with the TOPICA code showed that the parallel electric field extend even to the PL surrounding the antennas (see [29]), increasing the possibility of magnetic connection between areas with RF sheaths-enhanced voltages and the divertor entrance. It is then more than likely that RF sheaths play a role in the here described impurity increase. Nevertheless, to explain the interaction with recessed areas shown by the lasting effect of the Be evaporation, another explanation is needed. The role of fast neutrals is a possibility, although an initial quantification based on H and D fast neutral analysis showed that for the energy range of up to 30keV, the fast particle analyzer data was favoring higher W release by charge exchange particles in the case of NBI heating (see [29]). Transport modelling of these ICRF and NBI heated plasmas is also being done but so far, core transport indicates that only a higher W source can explain the higher W content in the plasma [33].

4. LOWER HYBRID CURRENT DRIVE

4.1. MODIFICATIONS FOR OPERATION IN THE ILW

The main modification to the LHCD launcher (Fig.5) was the change of the protective frame to

Be. The grill itself, made of Cucoated stainless steel, was unchanged. The launcher position was adjusted following photographic measurements and hot spot studies which showed that its position was 19mm forward of that indicated by the launcher position sensor. The first challenge when applying LHCD with the metallic wall was to avoid the potentially damaging heat flux due to the generation of fast electrons in front of the launcher, that can lead to very localised heat loads on magnetically connected PFCs. This phenomenon was quantified with the C-wall and the maximum heat flux projected onto the tile surface was estimated ~ 7MW/m^2 in worst case conditions [24]. The second challenge was arc detection, which can eventually lead to plasma disruptions due to high impurity influxes [34]. In order to further study the LH related hot-spots, protect Be components and develop new arc detection scheme, a dedicated viewing system (referred to as KL10) consisting of an IR camera, a visible camera and of 4 pyrometers was installed to monitor the LH launcher.

4.2. OPERATIONAL EXPERIENCE WITH THE ILW

The LH power was gradually increased up to 2.5MW staying within the maximum allowed (15MW/m^2 ~ 180kW per klystrons) in absence of a fully developed dedicated protection viewing systems. No specific impurity increase was observed. Good coupling as with the Cwall, was ensured by injecting D2 gas from GIM6 and, so far, no degradation compared to the C-wall was observed [35]. Unfortunately, due to delays in the KL10 commissioning, higher power could not be reached during the first ILW campaign. Nevertheless, by the end of the campaign, first IR camera observations were obtained, although absolute temperature values will only be available in the next campaigns, allowing proper documentation of launcher structure heating and fast electron hot-spots characterisation on PL3B. Note that in the conditions allowed so far, none of the LH related hot spots observed by the PIW were of a concern for the wall integrity. The first images from the visible camera highlighted the necessity to filter out visible light above 500nm to reduce the D_α line emission during D_2 injection from GIM6. A filter was also installed to remove Be lines. An example is shown on Fig.9 where, for the first time, the propagation of an arc can be seen in the case of an arc not extinguished early enough by the interlock system. So far 16 arc cases were seen by the camera (in 231 pulses). Most of the arcs were stopped by the existing arc detection system [34] but 4 were not stopped in time and led to plasma disruptions due to large Fe influxes. Development of a real-time arc detection system using bright spot detection which will complement the existing system is on-going.

5. SUMMARY AND OUTLOOK

Overall the use of NBI, ICRF and LH systems in the Be/W environment was very successful with efficient heating and no damage linked to the use of the heating power. This was the consequence of a cautious approach which has provided, in parallel with the development of the ITER-like wall protection systems, confidence in the safe application of the power. So far there are no obstacles preventing further increase of the power for the high performance scenario development programme [36]. Note that many of the issues discussed here have already been addressed for ITER. For

example, for the ITER 1MeV negative ion beams, the modeling shows that shine through will not be an issue [37]. For the ICRF, it is important to stress that the main chamber will be fully made of Be and that the antennas connection to the W divertor is minimized. Furthermore, the design team of the ITER ICRF antennas has used state of the art modeling tools that were not available at the time the A2's and particular attention was given to the grounding aspects of the antenna which, if not done properly, could lead to RF potentials on the antenna structures [38].

ACKNOWLEDGMENTS

This work, supported by the European Communities under the contract of Association between EURATOM and CCFE, was carried out within the framework of the European Fusion Development Agreement. The views and opinions expressed herein do not necessarily reflect those of the European Commission. This work was also part-funded by the RCUK Energy Programme under grant EP I501045

REFERENCES.

[1]. Duesing G., et al., Fusion Technology **11** (1987) 163.
[2]. Círíc, D., et al., Fusion Engineering and Design **82** (2007) 610.
[3]. Graham, M., et al., Plasma Physics and Controlled Fusion **54** (2012) 074011 .
[4]. Mayoral, M.-L., et al., 36th EPS Conference on Plasma Phys. Sofia, ECA Vol.33E, O-4.048 (2009).
[5]. Philipps V., et al., Fusion Engineering and Design **85** 20101581.
[6]. Durodie, F., et al. , Plasma Physics and Controlled Fusion **54** (2012) 074012.
[7]. Lennholm, M., et al, Proc. 16th Symp. on Fusion Engineering (Urbana–Champaign, IL) 1 (1995) 754.
[8]. Schild, Ph., et al., Proc. 17th Symp. on Fusion Engineering (San Diego, CA) 1 (1997) 421.
[9]. Ekedahl, A., et al., Plasma Physics and Controlled Fusion **51** (2009) 044001.
[10]. Matthews, G.F., et al., 20th International PSI Conference (2012), submitted to Journal of Nuclear Materials
[11]. Círíc, D., et al., Fusion Engineering and Design **86** (2011) 509.
[12]. JET-ITER support Programme/ programmatic document **4** (2004)
[13]. Strachan, J., et al., 38th EPS Conference on Plasma Physics, Vol. **35**G, PD2.12 (2011).
[14]. Arnoux G., et al, accepted for publication in Review of Scientific Instruments
[15]. Heikkinen J.A. and Sipilä S.K., Physics of Plasmas **2**, (1995) 3724/
[16]. MayoralL, M.-L., et al., 19th Topical Conf. on RF power in Plasmas, AIP Conf. Proc. 1406 (2011), 253.
[17]. Maggi, C.F., et al., 39th EPS Conference & 16th Int. Congress on Plasma Physics O3.108 (2012).
[18]. Lancellotti, V., et al., Nuclear Fusion **46** (2006) S476.

[19]. Van Eester, D., et al., 39th EPS Conference & 16th Int. Congress on Plasma Physics P1.094 (2012).
[20]. White R.B., et al. , Physical Review Letters **60** 1 (1988) 2038
[21]. Pütterich, T., et al., Nuclear Fusion **50** (2010) 025012. Pütterich, T., this conference
[22]. D'Ippolito, D.A., and Myra, J.R. Journal of Nuclear Materials **415** (2011) S1001.
[23]. Thomas Jr. C.E., et al., Journal of Nuclear Materials **220-222** (1995) 531
[24]. Jacquet, P. al., Nuclear Fusion **51** (2011) 103018.
[25]. Jacquet, P. al., 20th International PSI Conference (2012), submitted to Journal of Nuclear Materials.
[26]. Czarnecka A. et al., Plasma Physics and Controlled Fusion **54** (2012) 074013.
[27]. Czarnecka A. et al., 39th EPS Conference & 16th Int. Congress on Plasma Physics P5.047 (2012).
[28]. Klepper, C.C., et al., 20th International PSI Conference (2012), submitted to Journal of Nuclear Materials
[29]. Bobkov, Vl.V., et al., 20th International PSI Conference (2012), submitted to Journal of Nuclear Materials
[30]. Van Rooj, G.J., et al., EX/P5-05, this conference.
[31]. Bobkov, Vl.V., et al, Nuclear Fusion **50** (2010) 035004 .
[32]. Wukitch, S.J., et al. ,**390–391** (2009), 951.
[33]. Kalupin D, et al., TH/P2-01, this conference
[34]. Goniche M., et al., lasma Physics and Controlled Fusion **54** (2012) 074002
[35]. Kirov K., et al., 39th EPS Conference & 16th Int. Congress on Plasma Physics P1.092 (2012).
[36]. Joffrin E., et al., EX/1-1, this conference.
[37]. Oikawa,T., et al., 34th EPS Conference on Plasma Phys. Warsaw, Vol.31F, P-4.163 (2012).
[38]. Durodie, F., et al., ITR/P1-08, this conference.

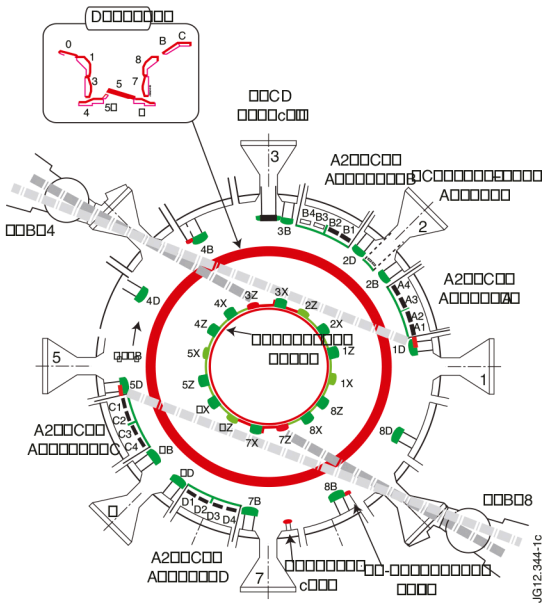

Figure 1: JET top view showing the heating systems layout. Areas with W or W-coated CFC tiles are colored in red and Be/Be-coated Inconel ones in dark/ light green, respectively. For more info see [5]. Outer limiters are referred to as PL (poloidal limiter) and inner limiters as IWGL (Inner wall guard limiter).

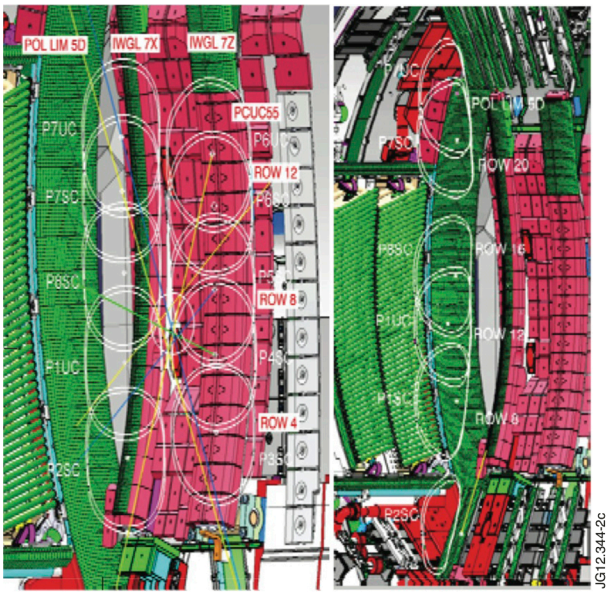

Figure 2: Beam footprints on the inner wall for normal and tangential bank (left) and on the outer wall for tangential bank (right). Contours are for power densities of 1 and 0.5MW/cm². W-coated CFC tilesare in red and Be bulk tiles in green.

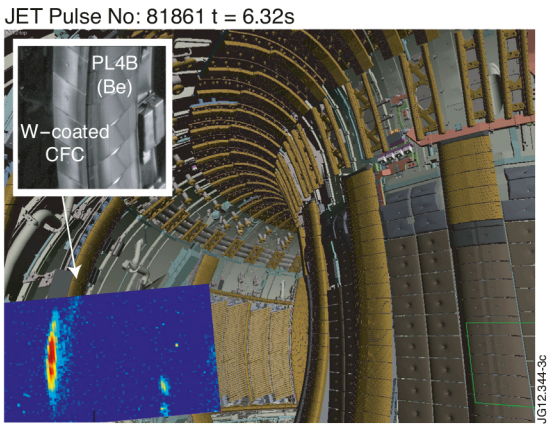

Figure 3: IR image of PL4B re-ionisation tiles heating from an outer limiter pulse with 5MW of NBI (Pulse No: 81861). The maximum hot spot temperature was 870°.

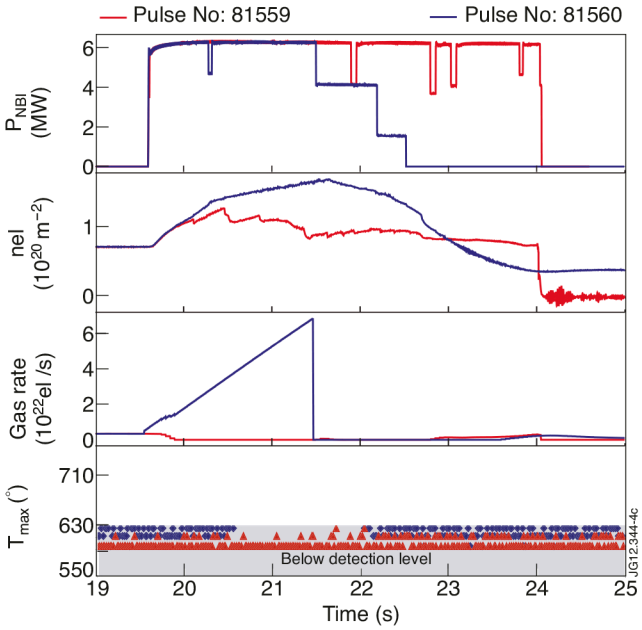

Figure 4: NBI power, line averaged central density, gas injection and maximum temperature for two pulses differing by the level of gas injected.

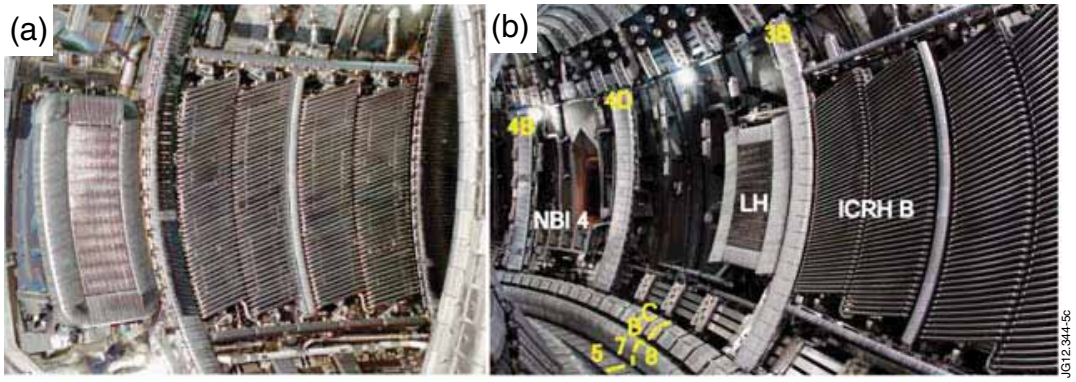

Figure 5: Inside view of JET (a) pre 2011; and (b) in 2011

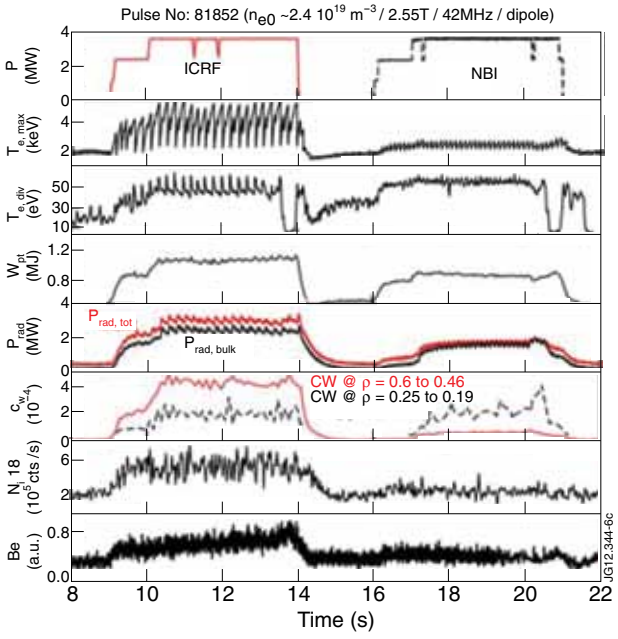

Figure 6: ICRF and NBI power, central T_e, divertor T_e, plasma energy, radiated power (total and bulk), W concentration [21], Ni18 and Be line emission. For this pulse, the low density was deliberately chosen to maximise the W influx.

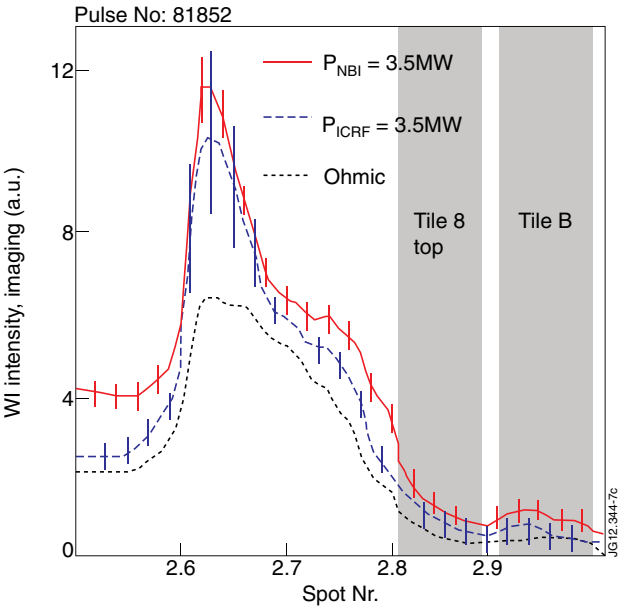

Figure 7: WI emission from WI imaging for ohmic, ICRF and NBI phases. W fluxes range are 3.10^{17} m^2s^{-1} from the top of tile 8 and 5.10^{17} m^2s^{-1} averaged over the strike point region (see [29]).

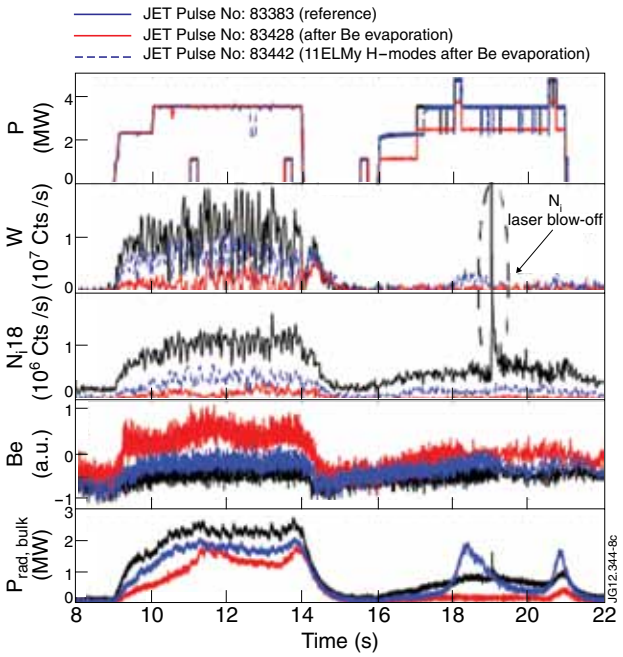

Figure 8: NBI and ICRF power; W, Ni18, and Be line emission; bulk radiated power for pulses before and after a Be evaporation. Note of possible offsets in the absolute W levels due to the differing Ni contamination for each pulse.

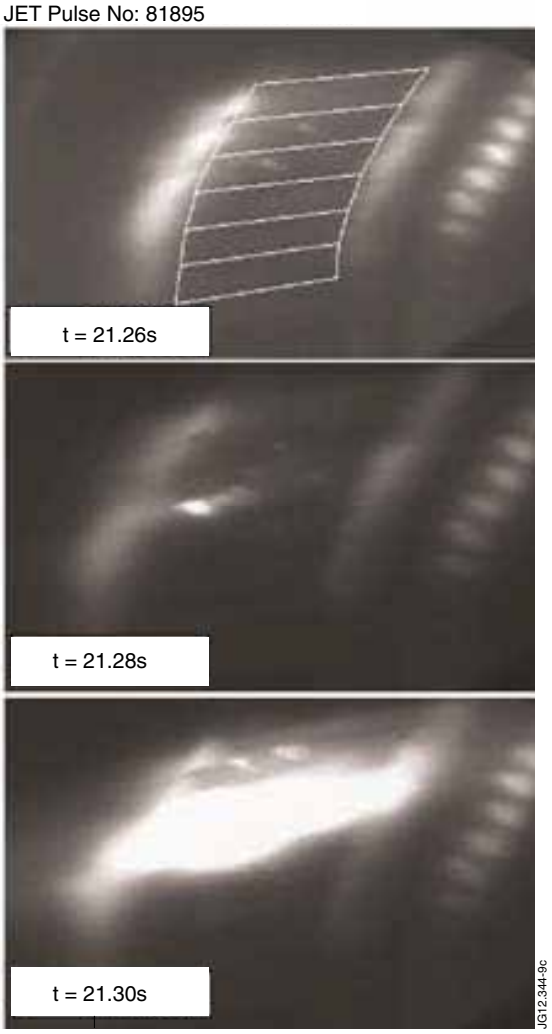

Figure 9: Observation of an arc propagating on the LH structure with the new visible camera.